perimentally found in Ref. [23] – our calculations suggest the prevalence of an AFM order. When Mn distributes both in the 6*c* of the QLs and SLs, which is the case of our samples according to our structure refinements, our calculations identify the FM phase as the ground state.

D. XAS and XMCD Data

To study the surface magnetic properties, we have performed x-ray absorption spectroscopy (XAS) measurements in the total electron yield (TEY) mode, which is element specific and has a probing depth on the nanometer scale. Measurements at the Bi $N_{4,5}$ edges (Fig. S7b) exhibit no XMCD. More interestingly, there is no XMCD at the Te $M_{4,5}$ edges either (Fig. S7a), which is in contrast to results in the closely related V- and Cr-doped $(Bi,Sb)_2Te_3$ [39–42], and which might indicate differences in the magnetic interactions of both compounds.

Next we focus on the Mn $L_{2,3}$ edge. Due to the shallow escape depth, the topmost SL contributes the most to the signal. However, even for SL termination, the FM Mn sheet is buried about 0.55 nm below the surface, and significantly more for QL termination. Therefore, probing depth effects have to be considered, when interpreting the ordered magnetic moments obtained with XMCD (see secs. II F and III). Fig. 4a compares XAS spectra measured with x-rays of opposite circular polarization at $T \approx 3.5\,\mathrm{K}$ and a magnetic field of $\mu_0 H = 0.15\,\mathrm{T}$ along the surface normal; the bottom green line showcases the substantial XMCD signal. In the inset we show that the peak remanent XMCD signal scales inversely with θ, where θ is the angle between the magnetization direction and the x-ray beam. This decline of XMCD is a strong indication of an out-of-plane easy axis for the Mn moments.

In Fig. 4b we show the magnetization obtained by measuring the peak L_3 XMCD signal at $T \approx 3.5\,\mathrm{K}$ within a field range of $\pm 0.3\,\mathrm{T}$. It exhibits a substantial remanence at $\mu_0 H = 0\,\mathrm{T}$, in sharp contrast to $MnBi_2Te_4$, which exhibits no remanent magnetization, and $MnBi_4Te_7$, which has a smaller remanence-to-saturation ratio [26]. Furthermore, we observe a coercive field of $\mu_0 H_c = 45\,\mathrm{mT}$. We caution against overinterpreting the similarity of this H_c with the bulk one: First, the data were measured at somewhat different temperatures, which has an effect on H_c (Fig. 2). Second, different ramping speeds were used, which, too, has an effect on H_c for magnetic TIs [43]. In addition, the hysteretic behavior of surface and bulk might be intrinsically different.

Finally, in Fig. 4c we compare the T-dependent remanent peak L_3 XMCD signal measured with surface sensitive TEY with the one measured with bulk sensitive total fluorescence yield (FY). Within the precision allowed by the T increments of 2 K, the transition temperatures at surface and bulk are consistent. We remark that the transition behavior as observed with SQUID and XMCD could differ somewhat due to the different measurement protocols: For XMCD, each point in Fig. 4c was obtained after driving to $\mu_0 H = 3\,\mathrm{T}$ and back to remanence. In contrast, in SQUID measurements a conventional FC protocol at 10 mT was used.

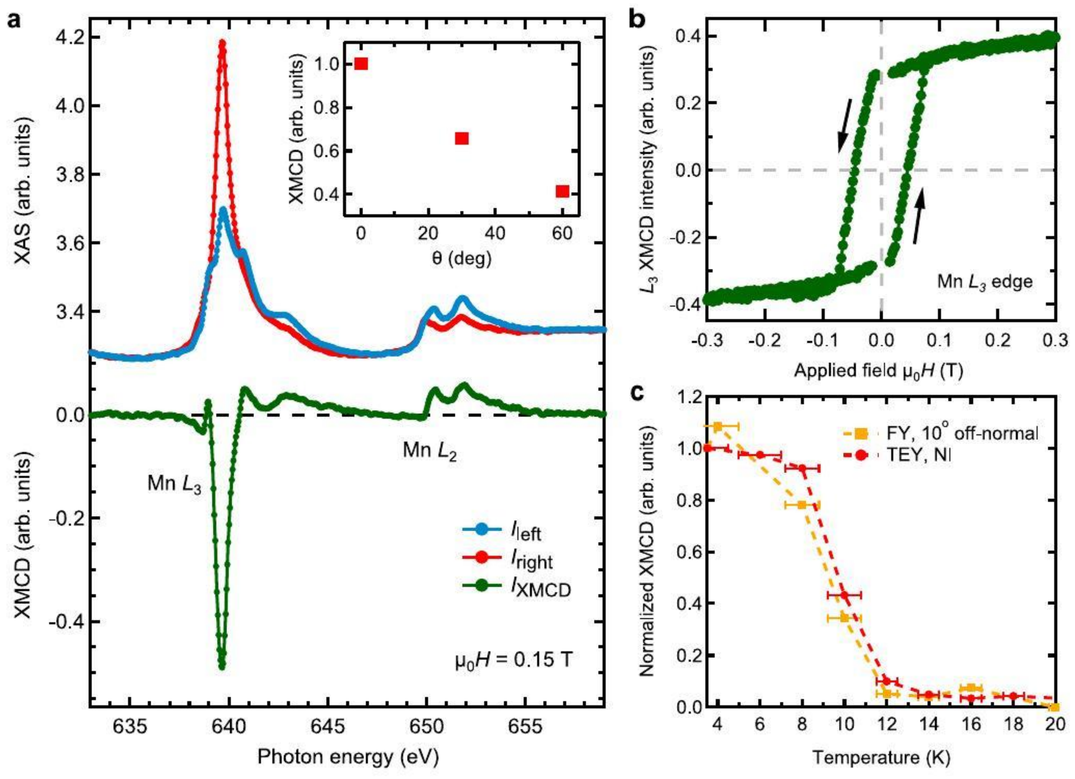

FIG. 4. X-ray spectroscopy data. (a) Mn $L_{2,3}$ edge XAS data for sample #4 obtained with left (I_{left}, blue) and right (I_{right}, red) circularly polarized light in normal incidence at $T \approx 3.5$ K in a magnetic field of 0.15 T. The corresponding XMCD signal $I_{\mathrm{XMCD}} = I_{\mathrm{left}} - I_{\mathrm{right}}$ is plotted below in green. The inset shows the angular dependence of the normalized remanent XMCD signal. (b) Magnetization curve of sample #4 ($I_{\mathrm{right}} - I_{\mathrm{left}}$) at $T \approx 3.5\,\mathrm{K}$, obtained as the Mn L_3 edge XMCD signal normalized by the XAS signal. (c) Temperature dependence of the remanent XMCD signal for sample #2 at the Mn L_3 edge measured at normal incidence in TEY mode (red) and 10° off normal incidence in FY mode (orange).

E. MLFT Calculations

The line shapes of the XAS and XMCD spectra contain important physical information, such as the *d*-electron configuration, including the local magnetic moments. Therefore, we have modeled our experimental data by MLFT (multiplet ligand-field theory). In our approach [39, 44–46] (sec. IV), rather than relying on oversimplified approximations, we adjust most of the MLFT parameters to the data and obtain $10Dq = 0.06$, $10DqL = 2T_{pp} = 1.9$, $\Delta = 1.1$, $U_{dd} = 4.0$, $U_{pd} = 5.0$, $V_{e_g} = 1.3$ and $V_{t2_g} = 0.65$ (all in units of eV). For the SO coupling constants, we use the Hartree-Fock values [47], whereas the Slater integrals are calculated based on DFT in the local density approximation (LDA, table I).

The calculated spectra (Fig. 5) show an excellent agreement with the experimental data, most notably for the XMCD, reproducing all the multiplet features and their relative energy positions. Whereas the nominal Mn^{2+} d^5 configuration ($^6S_{5/2}$) dominates with 71%, there is significant charge transfer from the Te ligands, resulting in a 27% contribution of $d^6\underline{L}$ to the ground state ($d^7\underline{L}^2$ contributes negligibly, see the inset in Fig. 5b). This hints towards a considerable hybridization between